Structure, dynamics, and thermodynamics of a family of potentials with tunable softness

Zane Shi,[1] Pablo G. Debenedetti,[2,a)] Frank H. Stillinger,[3] and Paul Ginart[2,b)]
[1]*Department of Physics, Princeton University, Princeton, New Jersey 08544, USA*
[2]*Department of Chemical and Biological Engineering, Princeton University, Princeton, New Jersey 08544, USA*
[3]*Department of Chemistry, Princeton University, Princeton, New Jersey 08544, USA*

(Received 2 June 2011; accepted 3 August 2011; published online 29 August 2011)

We investigate numerically the structure, thermodynamics, and relaxation behavior of a family of $(n, 6)$ Lennard-Jones-like glass-forming binary mixtures interacting via pair potentials with variable softness, fixed well depth, and fixed well depth location. These constraints give rise to progressively more negative attractive tails upon softening, for separations greater than the potential energy minimum. Over the range of conditions examined, we find only modest dependence of structure on softness. In contrast, decreasing the repulsive exponent from $n = 12$ to $n = 7$ causes the diffusivity to increase by as much as two orders of magnitude at fixed temperature and density, and produces mechanically stable packings (inherent structures) with cohesive energies that are, on average, $\sim$1.7 well depths per particle larger than for the corresponding Lennard-Jones ($n = 12$) case. The softer liquids have markedly higher entropies and lower Kauzmann temperatures than their Lennard-Jones ($n = 12$) counterparts, and they remain diffusive down to appreciably lower temperatures. We find that softening leads to a modest increase in fragility. © *2011 American Institute of Physics*. [doi:10.1063/1.3627148]

I. INTRODUCTION

Understanding the microscopic origin of the pronounced temperature dependence of structural relaxation in supercooled liquids, and the laboratory glass transition to which this behavior gives rise, is a major open question in condensed matter physics (see, e.g., Refs. 1–16). An important aspect of this question is elucidating how specific features of molecular interactions, such as attractive and repulsive forces, influence the rich variety of phenomena associated with the glass transition.[17] Computer simulations are ideally suited to the pursuit of this question because they allow interactions between particles to be varied in a systematic manner, thereby enabling the investigation of the effects of changes in individual variables to be conducted with a level of specificity not generally possible in experiments.

To date, relatively few investigations have explored systematically the effects of changes in the interaction potential upon viscous liquid behavior. Bordat *et al.*[18,19] investigated the dynamics of three different binary mixtures: the Kob-Andersen Lennard-Jones mixture[20] (80%A, 20%B, $\epsilon_{AA} = 1.0$, $\epsilon_{BB} = 0.5$, $\epsilon_{AB} = 1.5$, $\sigma_{AA} = 1.0$, $\sigma_{BB} = 0.88$, and $\sigma_{AB} = 0.8$), and the two variants thereof in which the AA interaction potential had repulsive and attractive exponents of (8, 5) and (12, 11), respectively, while the well depth and its location remained fixed. The anharmonicity of the pairwise interaction energy is largest for the (8, 5) case and smallest for the (12, 11) model, with the Kob-Andersen mixture falling in between. These authors found a positive correlation between fragility,[21] a measure of the sensitivity of the structural relaxation time to changes in temperature, and the anharmonicity of the interaction potential. Berthier and Tarjus[17,22] investigated the effect of attractive forces in viscous liquids by comparing the structure and dynamics of the Kob-Andersen binary Lennard-Jones mixture to those of the corresponding Weeks-Chandler-Andersen[23] purely repulsive mixture, which lacks the attractive tail. These authors found that at liquid-like densities and at temperatures characteristic of viscous liquid behavior, the dynamics is strongly influenced by the attractive forces. Michele *et al.* investigated the scaling of the dynamics of soft spheres upon varying the repulsive exponent, and found that the temperature dependence of the diffusivity collapses onto a universal curve upon rescaling the temperature.[24] It has recently been shown experimentally that colloidal particles exhibit decreasing fragility with increasing softness,[25] in apparent contradiction with the computational studies of Bordat *et al.* Krekelberg *et al.*[26] investigated the effects of short-range attractions on fluid structure and dynamics by comparing the properties of the hard-sphere and square-well systems. Pond *et al.*[27] compared the applicability of the generalized entropy-scaling approach[28,29] for estimating transport properties in several repulsive models (soft-sphere, Gaussian,[30] and Hertzian[31]). In addition to the above-mentioned studies, in which explicit perturbations of the interparticle interactions were investigated, it should also be mentioned that the accepted liquid-state picture whereby repulsive forces play a dominant role in determining the structure, with attractive forces providing a uniform cohesive background,[23] underlies important recent work on

a)Author to whom correspondence should be addressed. Electronic mail: pdebene@princeton.edu.
b)Present address: School of Medicine, University of Pennsylvania, Philadelphia, Pennsylvania 19104, USA.

viscous liquids. This includes the successful temperature and density scaling of supercooled liquid dynamics (e.g., Refs. 32–36), and a promising picture of liquid-state regularities based on the notion of strong pressure-energy correlations (e.g., Refs. 37–41).

It appears useful, in light of the above-cited work, to formulate models in which the specific aspects of interparticle interactions can be systematically perturbed, and to investigate the consequences of such perturbations on structure, dynamics, and thermodynamics, with emphasis on supercooled states. This is the task that we undertake here. Specifically, we construct a family of generalized Lennard-Jones binary mixtures with tunable softness, fixed well depth, and fixed well location. We investigate computationally a broad spectrum of the thermodynamic and dynamic properties as a function of softness. In Sec. II, we define the model and provide details of the computational methods utilized in our investigation. The thermodynamic properties of the family of mixtures are presented and discussed in Sec. III, and the corresponding analysis for dynamic properties is the subject of Sec. IV. The principal conclusions and suggestions for further inquiry are presented in Sec. V.

II. METHODS

A. Definition of potentials

Starting from the well-known (12, 6) Lennard-Jones (LJ) potential,

$$\phi^{\mathrm{LJ}}(r) = 4\epsilon\left[\left(\frac{\sigma}{r}\right)^{12} - \left(\frac{\sigma}{r}\right)^{6}\right], \tag{1}$$

we define, for a given repulsive exponent n, a generalized $(n, 6)$ potential with the following functional form:

$$\phi = 4\epsilon\left[\lambda\left(\frac{\sigma}{r}\right)^{n} - \alpha\left(\frac{\sigma}{r}\right)^{6}\right], \tag{2}$$

where

$$\lambda = \frac{3}{2}\left(\frac{2^{n/6}}{n-6}\right), \qquad \alpha = \frac{n}{2(n-6)}. \tag{3}$$

λ and α are chosen such that the well depth and location of the minimum of the generalized $(n, 6)$ potentials coincide with the minimum of the standard (12, 6) LJ potential (Figure 1). The second and third derivatives of ϕ with respect to r, evaluated at $r = 2^{1/6}\sigma$, where $\phi'(r) = 0$, are given by

$$\sigma^2\phi''/\epsilon = 2^{2/3}\cdot 3n, \tag{4}$$

$$\sigma^3\phi'''/\epsilon = -2^{1/2}\cdot 3n(n+9). \tag{5}$$

Thus, we have a family of potentials of varying softness, with the repulsive exponent n as the tuning parameter, with all members of the family sharing identical characteristic energy and length. It is important to point out that the constraints of invariant energy and length scales (well depth and well depth location) give rise to progressively stronger attractive energies (more negative attractive tails) for $r > 2^{1/6}\sigma$ upon decreasing n (see Figure 1). Such constrained softening will be shown to have a pronounced effect, particularly on the energy of the liquid and its inherent structures.[42]

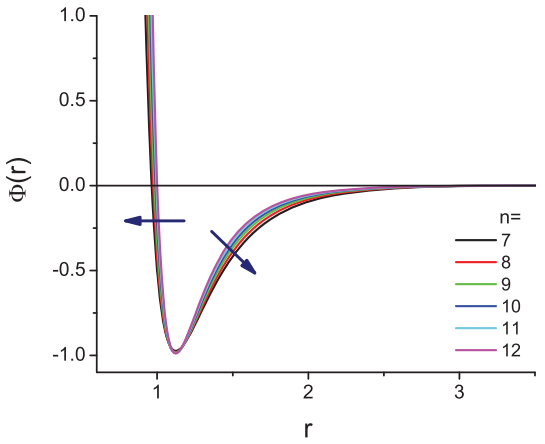

FIG. 1. The family of potentials used in this work. The arrows show the effect of softening.

In this study, we consider the family of potentials defined by Eq. (2), with $n = 7, 8, 9, 10, 11, 12$. Ahmed and Sadus[43] investigated solid-liquid equilibria in a family of potentials closely related to those used in this work. Several authors have investigated vapor-liquid coexistence in $(n, 6)$ or (n, m) potentials.[44–47] The usefulness of such models in the coarse-graining applications has also received attention.[47,48]

B. Simulation details

For each interaction potential, we study the well-known binary glass-forming mixture as parameterized by Kob and Andersen,[20] namely, a mixture of 80%A particles and 20%B particles, with parameters $\epsilon_{AA} = 1.0$, $\epsilon_{BB} = 0.5$, $\epsilon_{AB} = 1.5$, $\sigma_{AA} = 1.0$, $\sigma_{BB} = 0.88$, and $\sigma_{AB} = 0.8$. Both types of particles have the same mass, m. Throughout this paper, all quantities are expressed in reduced units: length in units of σ_{AA}, temperature in units of ϵ_{AA}/k_B, where k_B is the Boltzmann's constant, and time in units of $\sigma_{AA}(m/\epsilon_{AA})^{1/2}$. In order to ensure continuity of the potential and its first derivative at the potential cutoff (continuity needed for energy minimization calculations), we apply a shifted force correction to the potentials:

$$\phi^{sf}(r) = \begin{cases} \phi(r) - \phi(r_c) - (r - r_c)\phi'(r_c) & r \le r_c \\ 0 & r > r_c \end{cases}, \tag{6}$$

where $\phi(r)$ is the pair potential. To minimize the effects of the shift on the shape of the various potentials, we choose a rather large cutoff, $r_c = 3.5$. Our computational cell consists of 500 particles in a box of volume $V = (7.368)^3$, corresponding to a reduced density of $\rho = 1.25$. Periodic boundary conditions are applied in all directions. The velocity Verlet algorithm of numerical integration is used, and the molecular dynamics time step is 0.002. The system is initialized as an fcc lattice, where the identity of a particle is selected at random, while maintaining the overall 4 : 1 ratio of A to B particles, and is then melted at a high temperature of $T = 5.0$. It is then cooled to the desired temperature and equilibrated for 2.5×10^5 time

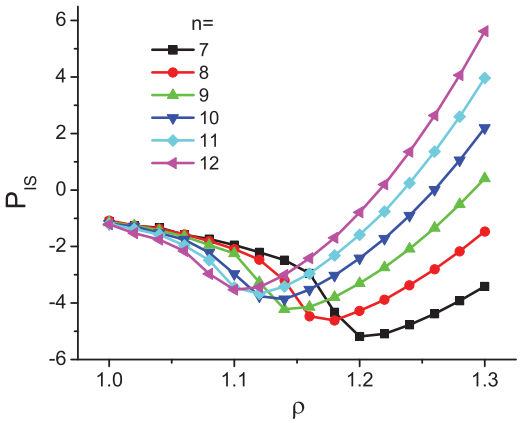

FIG. 2. Sastry curves showing the dependence of inherent structure pressure upon density. Each point is the average of 100 energy minimizations at constant volume starting from equilibrated liquid configurations at $T = 1.0$. Note the progressive destabilization of inherent structures upon softening, such that for $n = 7$, inherent structures with $\rho \leq 1.2$ are fractured and spatially inhomogeneous.

steps. A coordinate snapshot is taken at every 5000 time steps thereafter. The simulations are run at fixed particle number, total volume, and temperature (N, V, T), with a Nose-Hoover thermostat.[49]

To study the underlying inherent structures[42] embedded in the system's multidimensional energy landscape,[1] we perform energy minimization on each coordinate snapshot by applying the Fletcher and Reeves[50] method of conjugate gradients. The particles in the system are moved iteratively along the gradient of the potential energy landscape until $U(\mathbf{r}^N)$, the potential energy as a function of the system's $3N$ translational degrees of freedom, is at a local minimum. The criterion for convergence is satisfied when successive iterations reduce the energy per particle by less than 10^{-7}.

The simulation density of 1.25 is slightly higher than used in the earlier studies of the same 80-20 Kob and Andersen system interacting via the standard $(12, 6)$ LJ potential.[51] It was found that at a density of 1.2, a system interacting via the $n = 7$ potential cavitates upon isochoric energy minimization, creating fractures in the inherent structure configurations. The reason for this is apparent when we examine the so-called Sastry curves[52] for this family of potentials (i.e., the relationship between inherent structure pressure and density, also called the equation of state of the energy landscape[53])(Figure 2). The Sastry density, which corresponds to the minimum pressure along the curve, is the limit of mechanical stability of the inherent structures.[54] Below the Sastry density, fractures form in the inherent structure because the system cannot simultaneously satisfy mechanical stability and spatial homogeneity. Thus, as the interaction potential is softened, the inherent structures become mechanically unstable at progressively higher densities. We thus choose a density of 1.25 to ensure that the inherent structures are fracture-free for all values of the repulsive exponent used in this work.

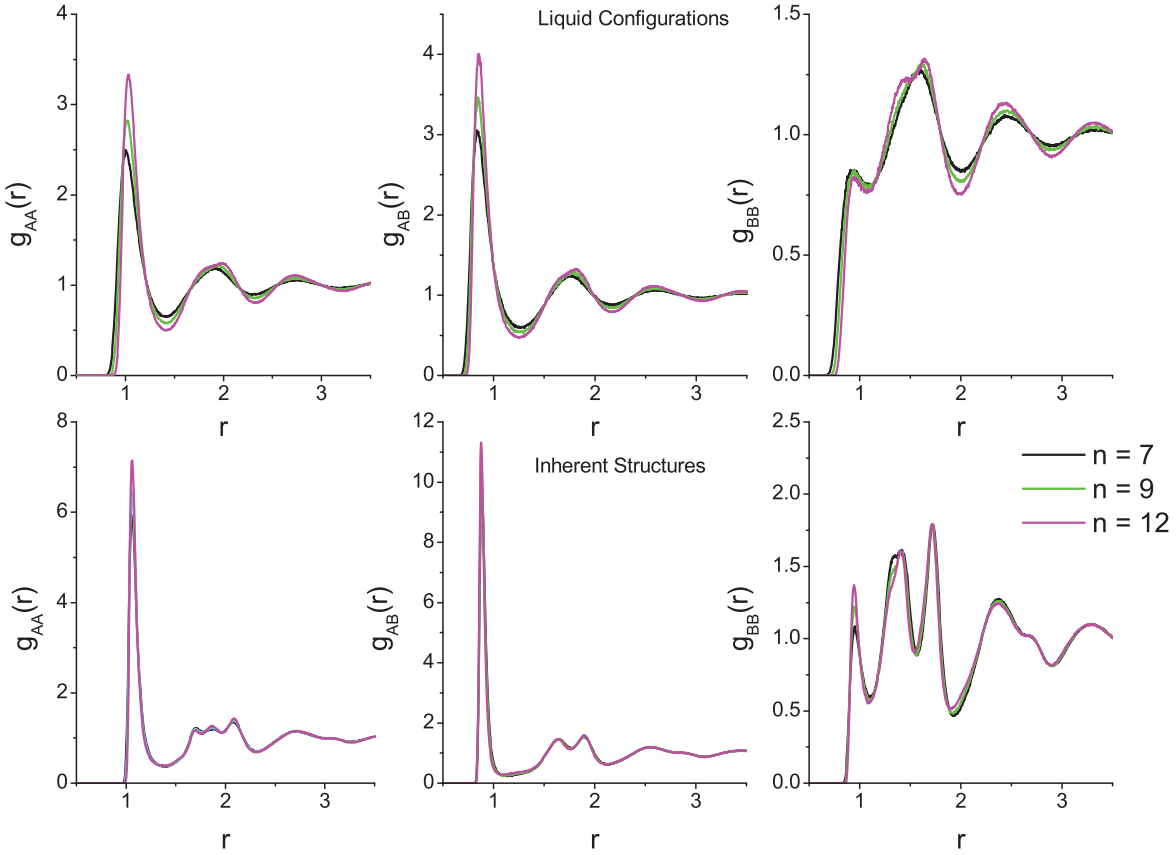

FIG. 3. The AA, AB, and BB radial distribution functions for both liquid configurations (top row) and inherent structures (bottom row) at $\rho = 1.25$, for three values of the repulsive exponent. The liquid configurations are equilibrated at $T = 1.2$; the inherent structures are obtained from the corresponding equilibrated liquids at $T = 1.2$.

III. RESULTS AND DISCUSSION: THERMODYNAMIC AND STRUCTURAL PROPERTIES

A. Radial distribution

For each of the six repulsive exponents considered, we calculate the three radial distribution functions, $g_{AA}(r)$, $g_{AB}(r)$, and $g_{BB}(r)$, for both liquid and inherent structure configurations. Representative results for $g_{AA}(r)$, $g_{AB}(r)$, and $g_{BB}(r)$ of the liquid configurations, equilibrated at $T = 1.2$, are shown in the top row of Figure 3, for exponents $n = 7, 9, 12$, and the corresponding inherent structure radial distribution functions are shown in the bottom row of Figure 3. It can be seen that radial distribution functions are very similar for the three exponents; the inherent structure curves are nearly identical, while the corresponding liquid configuration curves obtained before minimization exhibit only a modest dependence on n. Qualitatively similar results are obtained across the range of temperatures explored in this work ($0.3 \leq T \leq 2.0$). Thus, across the range of conditions investigated in this work, the softening of the interaction potential and the resulting increase in attractive energies beyond the potential minimum have only a modest effect on the liquid structure, and a negligible effect on the corresponding inherent structures. This is in contrast with several transport and thermodynamic properties reported in the following sections.

B. Energy

Figure 4 shows the equilibrium potential energy as a function of temperature for $n = 7, \ldots, 12$. The marked decrease in energy upon softening is in sharp contrast with the corresponding insensitivity of structure (compare Figures 3 and 4). Although surprising at first given that the family of potentials has fixed well depth by construction, the behavior shown in Figure 4 is a direct consequence of the progressively stronger attractions upon decreasing n (see Figure 1).

The same pronounced energetic stabilization upon softening of the potential (and the consequent increase in attractive energies beyond the potential energy minimum) can also be seen in the inherent structures (IS), as shown in Figure 5, where each point is the average of 2000 minimizations. Note that the lowest attainable mean inherent structure energy per particle decreases from -8.28 ($n = 12$) to -9.93 ($n = 7$). It is clear that the increase in attractive energies caused by softening allows the system to sample deeper basins in its energy landscape. In addition, the onset temperature, below which the depth of sampled inherent structures depends sensitively on the temperature at which the liquid is equilibrated prior to minimization, decreases upon softening. Thus, our constrained softening, which preserves the characteristic energy and length scales and thereby gives rise to enhanced attractions at separations exceeding the potential energy minimum, allows the system to more effectively sample its underlying energy landscape at fixed temperature. Equivalently, it enables the extension of liquid-like behavior to progressively lower temperatures. Indeed, a low temperature for $n = 12$ (e.g., $T = 0.55$; see Figure 5) still corresponds to a high temperature for $n = 7$.

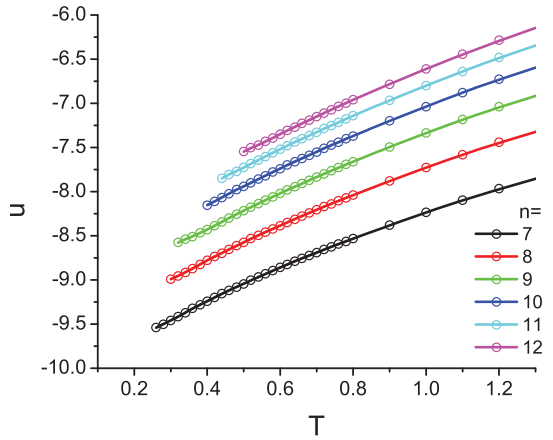

FIG. 4. Configurational energies per particle, for the equilibrated liquids at $\rho = 1.25$.

C. Entropy

We calculate the entropy associated with sampling different basins in the underlying energy landscape,[1] commonly referred to as configurational entropy, S_{conf}, in the literature on supercooled liquids.[55,56] Following the methodology of Sciortino and co-workers, we approximate this quantity as the difference between the entropy of the equilibrium liquid, S_{liq}, and the harmonic entropy of a disordered solid, S_{sol}. The later is obtained from the eigenfrequency spectrum of inherent structures generated from the equilibrium liquid at the given T and ρ.

The liquid entropy is calculated by thermodynamic integration. We begin with an ideal gas reference point ($T = 5.0$, $\rho = 0.01$), where the entropy is known, and integrate along the $T = 5.0$ isotherm to the density studied, $\rho = 1.25$, using the thermodynamic identity

$$S(T,\rho) = S_{ideal\ gas}(T,\rho) + \frac{U(T,\rho)}{T} + \int_{\infty}^{N/\rho} \frac{P_{ex}\mathrm{d}V'}{T}, \tag{7}$$

where U is the potential energy and P_{ex} is the excess pressure over the ideal-gas value at the same temperature and density. For a binary ideal gas mixture,

$$\frac{S_{ideal\ gas}(T,\rho)}{Nk_B} = -\frac{N_A}{N}\ln\left(\frac{N_A}{N}\right) - \frac{N_B}{N}\ln\left(\frac{N_B}{N}\right) + \frac{3}{2}\ln\left(\frac{mV^{2/3}}{\beta\hbar^2 2\pi}\right) - \ln N + \frac{5}{2}, \tag{8}$$

where N_A and N_B are the number of A and B particles, respectively, $N = N_A + N_B$, V is the volume, and $\beta = 1/k_BT$. The last integral in Eq. (7) is evaluated numerically (P_{ex} is calculated at discrete steps of the density ρ from 0.01 to 1.25 in steps of 0.01).

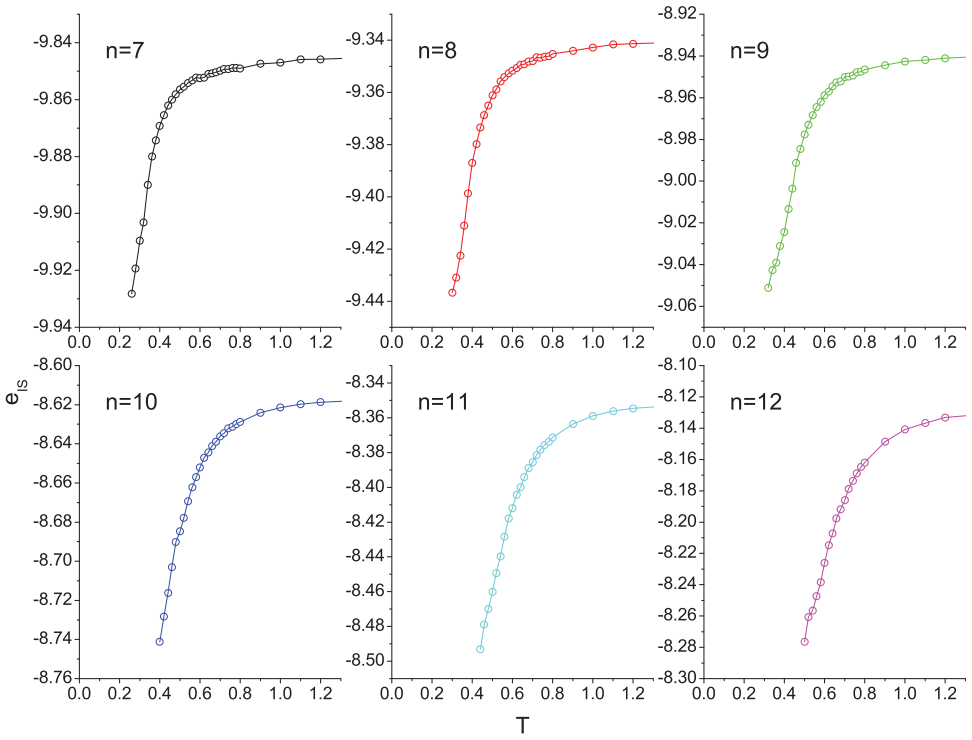

FIG. 5. Mean inherent structure energies as a function of the temperature prior to energy minimization, at $\rho = 1.25$, for the various potentials investigated in this work.

Once we have $S(T = 5.0, \rho = 1.25)$, we can then integrate along the isochoric path $\rho = 1.25$ to any temperature T:

$$S_{liq}(T, \rho = 1.25) = S(T = 5.0, \rho = 1.25) + \int_{T=5.0}^{T} \frac{C_V(T')}{T'} \mathrm{d}T', \qquad (9)$$

where $C_V(T) = (\partial U(T)/\partial T)_\rho + 3/2Nk_B$. For all the interaction potentials considered, we find that $U(T)$ obeys Rosenfeld-Tarazona scaling,[57] $U \sim T^{3/5}$ (Figure 6). This allows us to compute the integral in Eq. (9) analytically and provides a reliable extrapolation below the temperatures studied.

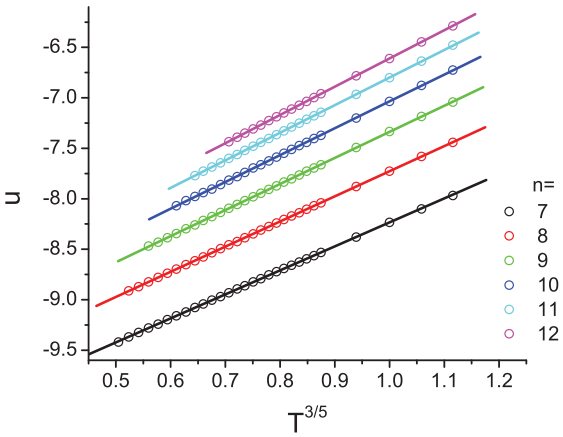

FIG. 6. Configurational energies of the equilibrated liquids plotted as a function of $T^{3/5}$. Lines are linear fits to the data, showing precise agreement with Rosenfeld-Tarazona scaling, $U \sim T^{3/5}$.

The entropy of the disordered solid, S_{sol} is computed by a normal mode analysis performed on the underlying inherent structures by applying the harmonic approximation:

$$S_{sol}(T, V) = \sum_{j=1}^{3N-3} [1 - \ln(\beta\hbar\omega_j)], \qquad (10)$$

where ω_j is the eigenfrequency of the jth normal mode. For each exponent n and temperature T, ω_j was calculated by evaluating the eigenvalues of the Hessian Matrix for 2000 inherent structure configurations. $\sum \ln \omega_j$ was then averaged over all configurations and used in Eq. (10) to calculate the solid entropy in the thermodynamic limit. We find that when the explicit T dependence is subtracted from S_{sol}, the resulting difference $S_{sol} - \ln T$ shows a weak T dependence and can be fitted to a simple quadratic function.[56] This fit allows us to also extrapolate S_{sol} to lower temperatures than those studied. To check the validity of the harmonic approximation applied here, we evaluate $u(T) - e_{\mathrm{IS}}(T) - 3/2k_BT$ for each of our potentials (Figure 7). This quantity vanishes for a harmonic system. It can be seen that in the range of temperatures for which entropy calculations were performed (see Figure 8), deviations from harmonic behavior are quite minor.

Figure 8 shows $s_{conf} = s_{liq} - s_{sol}$ as a function of temperature T, where $s = S/N$. We see that softening (lowering n) results in an appreciable increase in the configurational entropy for a given temperature. We also see a significant and systematic lowering of the Kauzmann temperature, T_K, defined by the condition[58] $s_{conf}(T_K) = 0$, as the softness of the interaction potential is increased. Furthermore, Figure 9 shows that the increase in the configurational entropy upon softening is not simply a result of a lower Kauzmann tem-

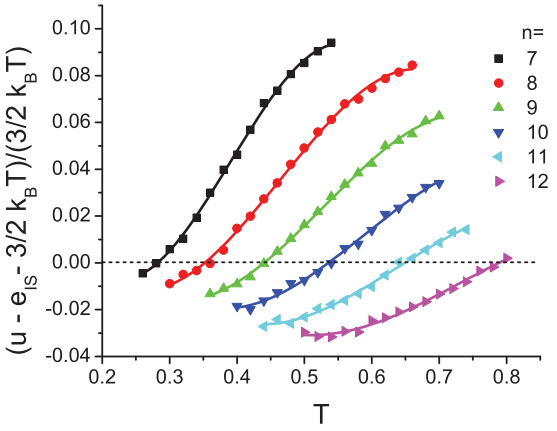

FIG. 7. Deviation of the difference between the average equilibrium configurational energy $u(T)$ and the average inherent structure energy, $e_{\rm IS}(T)$, and the corresponding quantity for a purely harmonic system, $3/2k_BT$

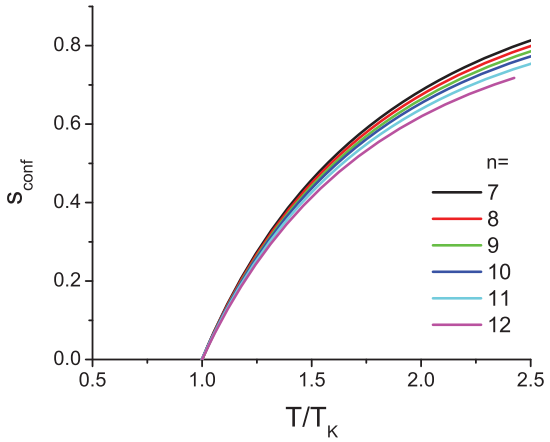

FIG. 9. Configurational entropies as a function of scaled temperature, at $\rho = 1.25$. The increase in configurational entropy upon softening is evident.

perature; when plotted as a function of T/T_K, s_{conf} increases more rapidly with the scaled temperature as the potential is softened. This shows that softening of the interaction potential results in an increase in the number of basins that the system samples, illustrating the fact that a modest change in the interaction potential has a pronounced effect on the system's low-temperature thermodynamics.

IV. RESULTS AND DISCUSSION: DYNAMIC PROPERTIES

A. Diffusion

For each repulsive exponent n, we calculate the diffusion coefficient using the standard Einstein equation:

$$D = \frac{1}{6}\lim_{t\to\infty}\frac{\mathrm{d}}{\mathrm{d}t}\langle\Delta r(t)^2\rangle, \tag{11}$$

where D is the diffusion coefficient and $\langle\Delta r(\tau)^2\rangle$ is the mean squared displacement of the particles after an interval of time τ. Figure 10 shows the diffusion coefficient of the A particles for the various potentials as a function of temperature. While we report here the diffusion results for A particles, we note that the diffusion properties of B particles are qualitatively similar. It can be seen that softening causes a pronounced increase in the diffusion coefficient, resulting in particles interacting via softer potentials to remain diffusive down to appreciably lower temperatures. The inset to Figure 10 shows the temperature at which $D = 10^{-4}$, as a function of n (the line though the D vs. T data is a simple logarithmic fit). Note that this characteristic temperature, like T_K (Figure 8, inset), decreases by a factor of 2 upon decreasing n from 12 to 7.

B. Self-intermediate scattering function

To further quantitatively describe the dynamics of the systems under consideration, we compute the self-intermediate scattering function (SISF) $F_s(k,t) = \langle\exp[i\mathbf{k}\cdot\Delta\mathbf{r}(t)]\rangle$, where $\Delta\mathbf{r}(t)$ is the displacement experienced by a particle in time t. This quantity, evaluated for A particles, is shown in Figure 11. The trajectory of

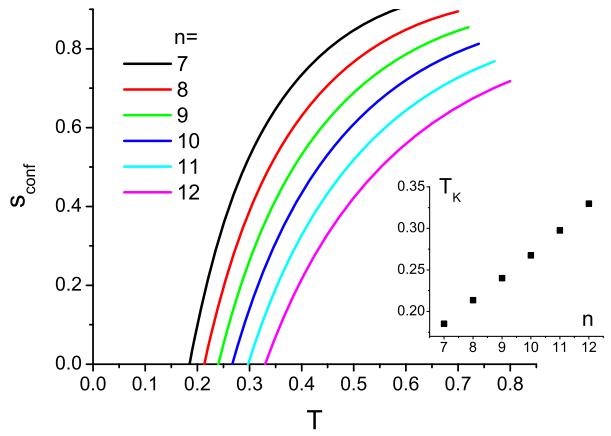

FIG. 8. Configurational entropies per particle as a function of temperature, at $\rho = 1.25$, for the various potentials investigated in this work. The inset shows the dependence of the temperature where $s_{conf} = 0$, upon the repulsive exponent.

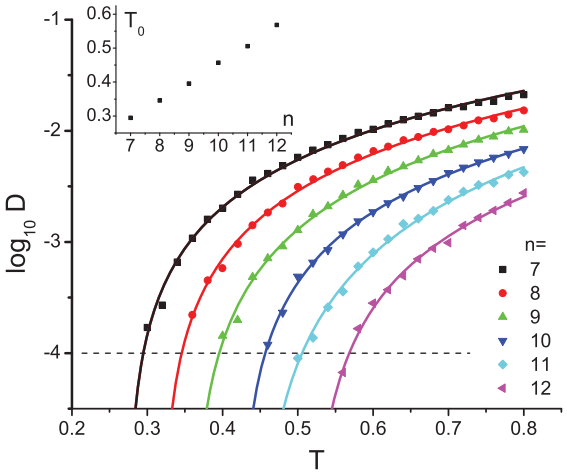

FIG. 10. Diffusion coefficients of A particles at $\rho = 1.25$, as a function of temperature, for the various potentials studied in this work. Lines are fits of the form $\log D = A + B\log(T + C)$. The inset shows the dependence of T_0, such that $D(T_0) = 10^{-4}$, upon the repulsive exponent.

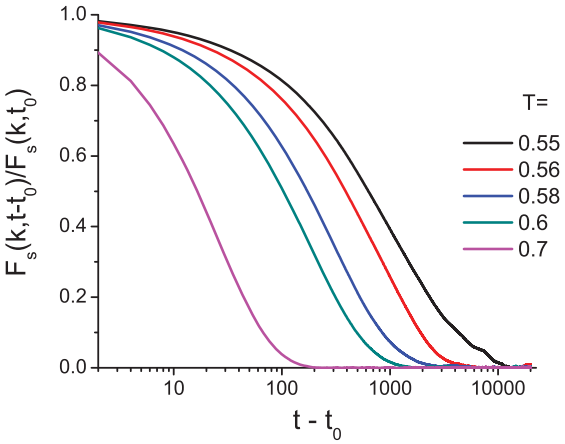

FIG. 11. Shifted and normalized self-intermediate scattering function for A particles, evaluated at $\rho = 1.25$ and $k = 7.28\sigma_{AA}^{-1}$, with $t_0 = 2.0$. The curves shown correspond to $n = 12$.

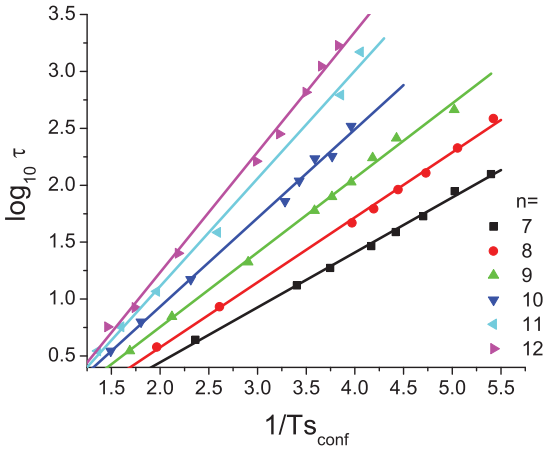

FIG. 13. Relationship between structural relaxation time obtained from the self-intermediate scattering function, and the configurational entropy. Linear fits to the data show good agreement with the Adam-Gibbs expression, Eq. (13).

the system was recorded for 1.5×10^7 times steps, with new time origins chosen every 1000 time steps, to provide independent "experiments" over which to average. The wave vector chosen is $k = 7.28\sigma_{AA}^{-1}$, which is close to the first peak of the static structure factor. We shift the time origin to $t_0 = 2.0$ to eliminate the Gaussian time dependence at short t, and normalize $F_s(k, t)$ to the value at t_0. We now define a relaxation time τ such that the shifted and normalized self-intermediate scattering function equals $1/e$.

Figure 12 shows the characteristic relaxation times as a function of temperature for the family of interaction potentials considered in this study. The solid lines are fits to the data using the Vogel-Tammann-Fulcher (VTF) equation,

$$\ln\left(\frac{\tau}{\tau_0}\right) = \frac{B}{T - T_{\mathrm{VTF}}}, \tag{12}$$

where T_{VTF} is the VTF singular temperature, τ_0 is the high-temperature limit of τ, and $k_B B$ is a characteristic energy (τ_0, T_{VTF}, and B were used as fitting parameters). For each exponent, the τ_0 obtained from fitting is of order 1. The VTF equation is used here simply as a fitting procedure, in order to extract the characteristic temperature where $\tau = 10^4$ (dashed line in Figure 12). This, as well as T_0 (Figure 10) and T_K (Figure 8) is used to investigate the dependence of fragility on the repulsive exponent n (see below). In general, for all of the repulsive exponents considered, the fit of the data to the VTF equation is quite good.

Figure 13 shows a linear relationship between the logarithm of the characteristic relaxation time, τ and the inverse of the configurational entropy multiplied by temperature, $1/Ts_{conf}$, calculated in Sec. III C. Thus, our systems behave in a manner that is consistent with the Adam-Gibbs equation:[59]

$$\tau(T) = A \exp\left(\frac{B}{Ts_{conf}(T)}\right), \tag{13}$$

where A and B are constants. This correspondence between dynamics and thermodynamics suggests that relaxation is influenced by the topography of the energy landscape.[51]

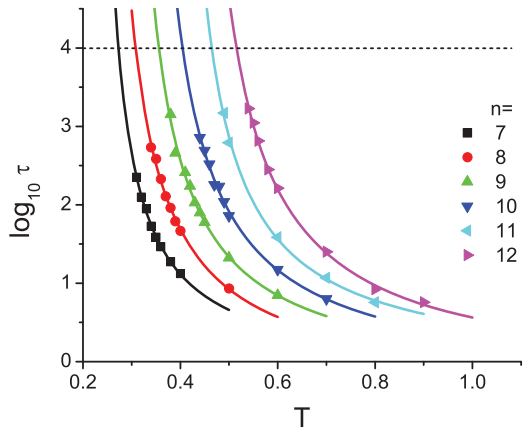

FIG. 12. Temperature dependence of the structural relaxation times at $\rho = 1.25$, obtained from the self-intermediate scattering function (Figure 11), using the condition $F_s(k, t - t_0)/F_s(k, t_0) = e^{-1}$. The lines are VTF fits (see text).

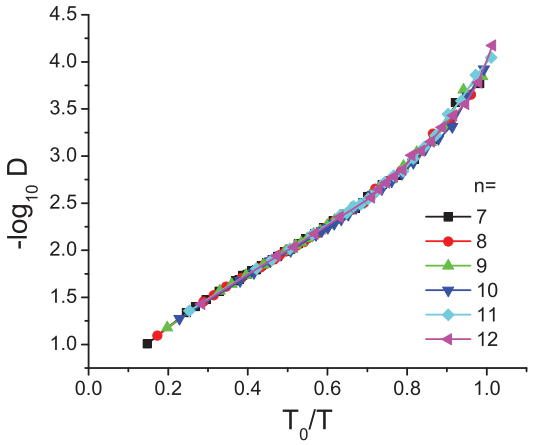

FIG. 14. Fragility plot using diffusion as a relaxation rate measure, at $\rho = 1.25$. The diffusion coefficients are for A particles (Figure 10), and T_0 is chosen such that $D(T_0) = 10^{-4}$.

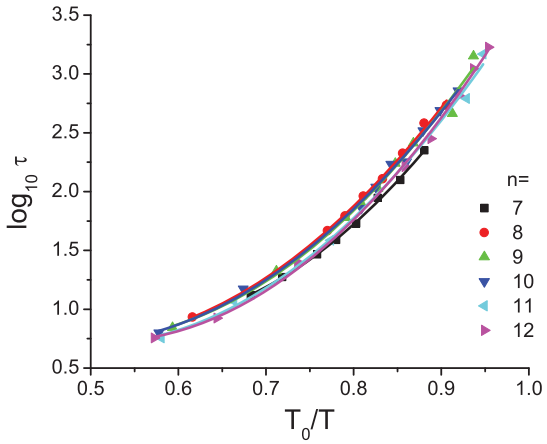

FIG. 15. Fragility plot using τ as a relaxation rate measure (see Figure 11), at $\rho = 1.25$. T_0 is chosen such that $\tau(T_0) = 10^4$ (see Figure 12).

C. Fragility

We now examine the effect of softening on the fragility of the family of glass formers. From Sec. IV A and IV B, we have two measures of relaxation rates for each repulsive interaction exponent: the inverse of the diffusion coefficient, $1/D$ and the characteristic time τ where $F_s(k, \tau) = 1/e$. These measures can be used to produce the Angell plot,[1,21] in order to compare the fragility of the systems under differing interaction potentials. For inverse diffusion, we choose the characteristic temperature, T_0^D, to be such that $D(T_0^D) = 10^{-4}$ (Figure 10). For the characteristic time based on the SISF, we investigate two characteristic temperatures: T_0^{SISF}, such that $\tau(T_0^{\mathrm{SISF}}) = 10^4$, and T_K.

Figures 14–16 are the resulting Angell plots. Figure 14 shows a clear collapse of all the curves, indicating no effect of softening on fragility when diffusivity is used as a measure of relaxation rate. It remains to be seen whether this trend persists when longer simulations at lower temperatures are used. A modest increase in fragility upon softening can be seen from Figure 15 if τ is used as a relaxation measure. Use of T_K as the characteristic temperature accentuates this trend (Figure 16), although the effect is not large. It should be noted

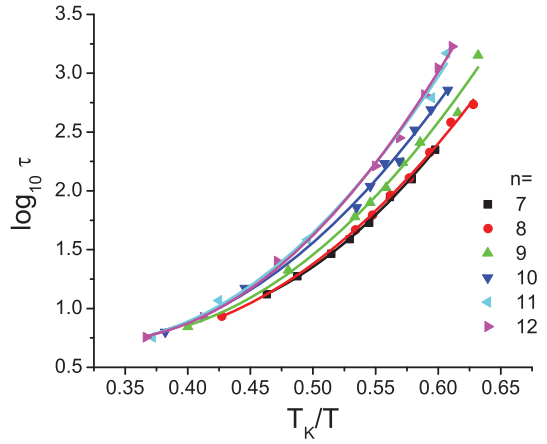

FIG. 16. Same as Figure 15, but using T_K as the characteristic temperature (see Figure 8).

though, that whereas in Figures 14 and 15 the attainable range of T_0/T is close to 1, the lowest scaled temperature attained in Figure 16 is 0.65.

Figures 14–16 thus illustrate not only a modest dependence of fragility upon constrained softening, but, more broadly, they point to a challenge inherent in calculating fragility computationally. This arises because, at the temperatures that can be sampled in MD simulations, the system is considerably farther away from the structural arrest than in the corresponding experimental determination of fragilities.

V. CONCLUSIONS

In this paper, we have investigated numerically the structural, thermodynamic and dynamic properties of a family of potentials of variable softness, and fixed well depth and well depth location. In order to explore the low-temperature non-crystalline behavior we considered, for each value of the repulsive exponent, a Kob-Andersen glass-forming binary mixture.[20] Simulations were conducted at a single density, chosen to be high enough to prevent cavitation even for the softest version of the potential investigated here.

Liquid structure, as described by the pair correlation functions, is only moderately sensitive to constrained variations in softness, and inherent structures are remarkably insensitive to such a perturbation. In sharp contrast, both dynamics and thermodynamics exhibit marked sensitivity to softness. Upon decreasing the repulsive exponent from 12 to 7, the translational diffusion coefficient increases by as much as two orders of magnitude, and liquids interacting via softer potentials remain diffusive down to appreciably lower temperatures. The average configurational energy per particle is larger in magnitude for the softer ($n = 7$) equilibrium liquid mixture than for the Lennard-Jones ($n = 12$) counterpart by more than two full well depths, reflecting the progressively stronger attractions that ensue upon constrained softening, while satisfying the fixed well depth and location constraints (Figure 1). Accordingly, the average inherent structure energies are appreciably more negative for the softer mixtures. The lowest-energy mechanically stable packings (inherent structures) that we were able to form, corresponding to the softer extreme considered here ($n = 7$), possess on average an additional cohesive energy of roughly 1.7 well depths per particle relative to their $n = 12$ counterparts (Figure 5). This is a consequence of the stronger attractive energies (more negative attractive tails) at separations greater than the well depth that arise as a result of softening.

Progressive softening also results in an increase in entropy, a decrease in the Kauzmann temperature, and a marked extension towards lower temperatures of the conditions at which equilibrium liquid behavior can be observed. Constrained softening, in other words, leads to enhanced entropy and mobility, more stable particle packings, and diffusive behavior at lower temperatures. We find only a modest increase in the fragility upon softening, and in order to uncover this trend it is necessary to use both extrapolated relaxation times and extrapolated characteristic temperatures. This points to the challenge of calculating fragilities by molecular-based

computer simulation, a challenge that originates with the difficulty of sampling low enough temperatures.

The rich behavior identified in the course of this research suggests several directions for future work. In light of the contrast of our results with experimental observations for colloidal particles[25] in which softening leads to a progressive decrease in fragility, it would be interesting to extend the present fragility calculations to other densities. This would allow exploration of regimes in which particles sample different regions of their respective pair potentials. More generally, extending the present structural, dynamic, and thermodynamic calculations to a broader range of conditions, including low-density states leading to cavitation in the softer models (Figure 2), is important in order to acquire a fuller picture of this family of potentials. It is also of interest to explore the possibility of scaling behavior, whereby physical properties for the various models may be collapsed into a single curve by appropriate scaling of temperature and/or density. The pronounced sensitivity of inherent structure energy to softness (Figure 5) may be of relevance in optimization problems, where strategies involving appropriately chosen cycles of softness perturbations might be useful for locating deep potential energy minima. Other families of models can be formulated, with an eye to introducing similar systematic perturbations of alternative aspects of the interaction potential, such as attractions. We plan to report our results on several of these topics in future papers.

ACKNOWLEDGMENTS

P.G.D. gratefully acknowledges the support of the Princeton Center for Complex Materials (National Science Foundation Materials Research Science and Engineering Center Grant No. DMR-0819860) and of the National Science Foundation (NSF) (Grant No. CHE-0908265).

[1] P. G. Debenedetti and F. H. Stillinger, Nature (London) **410**, 259 (2001).
[2] V. Lubchenko and P. G. Wolynes, Annu. Rev. Phys. Chem. **58**, 235 (2007).
[3] V. Lubchenko and P. G. Wolynes, J. Chem. Phys. **121**, 2852 (2004).
[4] J. P. Garrahan and D. Chandler, Proc. Natl. Acad. Sci. U.S.A. **100**, 9710 (2003).
[5] L. O. Hedges, R. L. Jack, J. P. Garrahan, and D. Chandler, Science **323**, 1309 (2009).
[6] J.-P. Bouchaud and G. Biroli, J. Chem. Phys. **121**, 7347 (2004).
[7] G. Biroli and J.-P. Bouchaud, J. Phys. Condens. Matter **19**, 205101 (2007).
[8] G. Biroli, J.-P. Bouchaud, A. Cavagna, T. S. Grigera, and P. Verrocchio, Nat. Phys. **4**, 771 (2008).
[9] R. K. Darst, D. R. Reichman, and G. Biroli, J. Chem. Phys. **132**, 044510 (2010).
[10] G. Tarjus, S. A. Kivelson, Z. Nussinov, and P. Viot, J. Phys. Condens. Matter **17**, R1143 (2005).
[11] A. Heuer, J. Phys. Condens. Matter **20**, 373101 (2008).
[12] A. Widmer-Cooper and P. Harrowell, Phys. Rev. Lett. **96**, 185701 (2006).
[13] A. Widmer-Cooper and P. Harrowell, J. Chem. Phys. **126**, 154503 (2007).
[14] E. J. Saltzman and K. S. Schweizer, J. Chem. Phys. **125**, 044509 (2006).
[15] J. S. Langer, Phys. Rev. Lett. **97**, 115704 (2006).
[16] J. C. Dyre, Rev. Mod. Phys. **78**, 953 (2006).
[17] L. Berthier and G. Tarjus, Phys. Rev. Lett. **103**, 170601 (2009).
[18] P. Bordat, F. Affouard, M. Descamps, and K. L. Ngai, Phys. Rev. Lett. **93**, 105502 (2004).
[19] P. Bordat, F. Affouard, M. Descamps, and K. L. Ngai, J. Non-Cryst. Solids **352**, 4630 (2006).
[20] W. Kob and H. C. Andersen, Phys. Rev. E **51**, 4626 (1995).
[21] C. A. Angell, K. L. Ngai, G. B. McKenna, P. F. McMillan, and S. W. Martin, J. Appl. Phys. **88**, 3113 (2000).
[22] L. Berthier and G. Tarjus, J. Chem. Phys. **134**, 214503 (2011).
[23] J. D. Weeks, D. Chandler, and H. C. Andersen, J. Chem. Phys. **54**, 5237 (1971).
[24] C. D. Michele, F. Sciortino, and A. Coniglio, J. Phys.: Condens. Matter **16**, L489 (2004).
[25] J. Mattsson, H. M. Wyss, A. Fernandez-Nieves, K. Miyazaki, Z. Hu, D. R. Reichman, and D. A. Weitz, Nature (London) **462**, 83 (2009).
[26] W. P. Krekelberg, J. Mittal, V. Ganesan, and T. M. Truskett, J. Chem. Phys. **127**, 044502 (2007).
[27] M. J. Pond, J. R. Errington, and T. M. Truskett, J. Chem. Phys. **134**, 081101 (2011).
[28] Y. Rosenfeld, J. Phys.: Condens. Matter **11**, 5415 (1999).
[29] W. P. Krekelberg, M. J. Pond, G. Goel, V. K. Shen, J. R. Errington, and T. M. Truskett, Phys. Rev. E **80**, 061205 (2009).
[30] F. H. Stillinger and T. A. Weber, J. Chem. Phys. **68**, 3837 (1978).
[31] L. Berthier, A. J. Moreno, and G. Szamel, Phys. Rev. E **82**, 060501 (2010).
[32] R. Casalini and C. M. Roland, Phys. Rev. E **69**, 062501 (2004).
[33] R. Casalini and C. M. Roland, Phys. Rev. E **72**, 031503 (2005).
[34] C. M. Roland, S. Hensel-Bielowka, M. Paluch, and R. Casalini, Rep. Prog. Phys. **68**, 1405 (2005).
[35] C. M. Roland, S. Bair, and R. Casalini, J. Chem. Phys. **125**, 124508 (2006).
[36] R. Casalini, U. Mohanty, and C. M. Roland, J. Chem. Phys. **125**, 014505 (2006).
[37] U. R. Pedersen, N. P. Bailey, T. B. Schrøder, and J. C. Dyre, Phys. Rev. Lett. **100**, 015701 (2008).
[38] N. P. Bailey, U. R. Pedersen, N. Gnan, T. B. Schrøder, and J. C. Dyre, J. Chem. Phys. **129**, 184507 (2008).
[39] N. P. Bailey, U. R. Pedersen, N. Gnan, T. B. Schrøder, and J. C. Dyre, J. Chem. Phys. **129**, 184508 (2008).
[40] T. B. Schrøder, N. P. Bailey, U. R. Pedersen, N. Gnan, and J. C. Dyre, J. Chem. Phys. **131**, 234503 (2009).
[41] T. B. Schrøder, N. Gnan, U. R. Pedersen, N. P. Bailey, and J. C. Dyre, J. Chem. Phys. **134**, 164505 (2011).
[42] F. H. Stillinger and T. A. Weber, Phys. Rev. A **25**, 978 (1982).
[43] A. Ahmed and R. J. Sadus, J. Chem. Phys. **131**, 174504 (2009); Ahmed and Sadus imposed the constraint of constant well depth but not the constraint of fixed well depth location. It can be shown, however, that the potentials used in this work and in that of Ahmed and Sadus can be mapped onto each other by rescaling σ.
[44] H. Okumura and F. Yonezawa, J. Chem. Phys. **113**, 9162 (2000).
[45] P. Orea, Y. Reyes-Mercado, and Y. Duda, Phys. Lett. A **372**, 7024 (2008).
[46] J. J. Potoff and D. A. Bernard-Brunel, J. Phys. Chem. B **113**, 14725 (2009).
[47] K. A. Maerzke and J. I. Siepmann, J. Phys. Chem. B **115**, 3452 (2009).
[48] X. He, W. Shinoda, R. DeVane, and M. L. Klein, Mol. Phys. **108**, 2007 (2010).
[49] W. G. Hoover, Phys. Rev. A **31**, 1695 (1985).
[50] R. Fletcher and C. M. Reeves, Comput. J. **7**, 149 (1964).
[51] S. Sastry, P. G. Debenedetti, and F. H. Stillinger, Nature (London) **393**, 554 (1998).
[52] S. Sastry, P. G. Debenedetti, and F. H. Stillinger, Phys. Rev. E **56**, 5533 (1997).
[53] P. G. Debenedetti, F. H. Stillinger, T. M. Truskett, and C. J. Roberts, J. Phys. Chem. B **103**, 7390 (1999).
[54] M. Utz, P. G. Debenedetti, and F. H. Stillinger, J. Chem. Phys. **114**, 10049 (2001).
[55] F. Sciortino, W. Kob, and P. Tartaglia, Phys. Rev. Lett. **83**, 3214 (1999).
[56] F. Sciortino, W. Kob, and P. Tartaglia, J. Phys.: Condens. Matter **12**, 6525 (2000).
[57] Y. Rosenfeld and P. Tarazona, Mol. Phys. **95**, 141 (1998).
[58] W. Kauzmann, Chem. Rev. **43**, 219 (1948). The temperature discussed by Kauzmann in his classic paper is that at which the entropies of the liquid and crystal phases of a given substance become equal. We use instead the common definition of the Kauzmann temperature in the contemporary literature on the glass transition, namely the temperature at which the entropy associated with the exploration of distinct configurations appears to vanish. As shown by us [F. H. Stillinger, P. G. Debenedetti, and T. M. Truskett, J. Phys. Chem. B **105**, 11809 (2001)], the former is experimentally attainable and is logically disconnected to the presence of an ideal glass transition.
[59] G. Adam and J. H. Gibbs, J. Chem. Phys. **43**, 139 (1965).